MR-based spatiotemporal anisotropic atrophy evaluation of hippocampus in AD progression by multiscale skeletal representation

Na Gao[1], Zhiyuan Liu[2], Yuesheng Deng[1], Hantao Chen[1], Chenfei Ye[3], Qi Yang[5,6,7], Ting Ma[1348*]

[1]The Department of Electronic & Information Engineering, Harbin Institute of Technology (Shenzhen), Shenzhen, China.

[2]Department of Computer Science, University of North Carolina at Chapel Hill, US

[3]International Research Institute for Artificial Intelligence, Harbin Institute of Technology at Shenzhen, Shenzhen, China

[4]Peng Cheng Laboratory, Shenzhen, China

[5]Department of Radiology, Beijing Chaoyang Hospital, Capital Medical University, Beijing 100020, China

[6]Key Lab of Medical Engineering for Cardiovascular Disease, Ministry of Education

[7]Beijing Advanced Innovation Center for Big Data-Based Precision Medicine

[8]Guangdong Provincial Key Laboratory of Aerospace Communication and Networking Technology, Harbin Institute of Technology (Shenzhen), Shenzhen, China

Corresponding author: Ting Ma. Phone: +86-755-26033608; fax: +86-755-26033608; e-mail: tma@hit.edu.cn

Na Gao: callie.gao@outlook.com

Zhiyuan Liu: zhiy@cs.unc.edu

Yuesheng Deng: 705501518@qq.com

Hantao Chen: htchenhitsz@outlook.com

Chenfei Ye: chenfei.ye@foxmail.com

Qi Yang: yangyangqiqi@gmail.com

Ting Ma: tma@hit.edu.cn

*Corresponding author and Lead Contact: Ting Ma, PhD

Department of Electronics and Information, Harbin Institute of Technology at Shenzhen, Shenzhen, Guangdong Province, China

Rm 1206, Information Building, HIT Campus, Shenzhen University Town

Nanshan District, Shenzhen

Guangdong Province, 518055

Tel: +86-755-26409293

Email: tma@hit.edu.cn

Running title: MEASURE AD-AFFECTED HIPPOCAMPAL ATROPHY

Keywords: Alzheimer's disease; MRI; Hippocampal morphology; Skeletal representations; Shape analysis.

Key points:

1. **The proposed method can comprehensively describe the hippocampal morphology and its atrophy with interpretable spatiotemporal measurements.**
2. **We find distinct trajectories in morphological changes of hippocampus between the amyloid-β positive progressive Mild Cognitive Impairment (pMCI) and stable Mild Cognitive Impairment (sMCI) patients in the prodromal stage of AD progression.**

3. This study narrows the gap between histological and 3T in-vivo imaging based findings.

Acknowledgments

We appreciate Professor Stephen M. Pizer (Department of Computer Science, University of North Carolina at Chapel Hill) and James Fishbaugh (Kitware, Inc.) for providing helpful advices for this study. We thank Ran Li for giving suggestions on plotting the figures. This study is supported by grants from the National Natural Science Foundation of P.R. China (62276081, 62106113), Innovation Team and Talents Cultivation Program of National Administration of Traditional Chinese Medicine (NO:ZYYCXTD-C-202004), Basic Research Foundation of Shenzhen Science and Technology Stable Support Program (GXWD20201230155427003-20200822115709001).

Declaration of Interests

The authors declare no competing interests.

Abstract

Increasing evidence have shown a higher sensitivity of Alzheimer's disease (AD) progression by local hippocampal atrophy rather than whole volume. However, neither the existing subfield-volume-based nor surface-based morphological method is capable to describe the comprehensive process of hippocampal atrophy as sensitive as histological findings. To map histological distinctive measurements onto medical MR images, we propose a multiscale skeletal representation (m-s-rep) to quantify focal hippocampal atrophy during AD progression on longitudinal cohorts. The m-s-rep describes large-to-small scale hippocampal morphology by spoke interpolation over label projection on skeletal models. To improve intra-subject morphological correspondence, we align the longitudinal m-s-reps by surface-based transformations from baseline to following timepoints. Cross-sectional and longitudinal measurements derived from the m-s-rep are statistically analyzed to comprehensively evaluate the bilateral hippocampal atrophy. Participates of amyloid-β positive (Aβ+) progressive mild cognitive impairment (pMCI, n=67), Aβ+ stable mild cognitive impairment (sMCI, n=88) and Aβ− normal controls (n=81) from ADNI are analyzed. Our results show that atrophy affected by pMCI is dominated by decrease of lateral-medial extent, with 1.8mm less lateral-medial width in two years preceding to conversion ($p<0.01$) and a maximum 3.05%/year more local atrophy rates in medial head ($p=0.011$) than controls during pMCI-to-AD conversion. Moreover, pMCI exhibits more severe and widespread atrophy in the hippocampal head and body than sMCI, with 1.21mm less thickness in medial head of the left hippocampus in two years preceding to conversion ($p=0.012$). In sum, our proposed method can quantitatively

measure the hippocampal morphological changes on 3T MRI images, potentially assisting AD pre-diagnosis and prognosis.

1 Introduction

Currently, the best-established structural imaging marker for early Alzheimer's Disease (AD) diagnosis is the hippocampal atrophy (Dubois et al., 2014; Frisoni et al., 2010; Hill et al., 2014), which is mostly quantified as volume decrease in clinical studies. However, the overall hippocampal volume has low specificality discriminating potential MCI-to-AD converters during AD prodromal stage (Lombardi et al., 2020; Ruchinskas et al., 2022; van Oostveen and de Lange, 2021). Evidence from AD pathology, histology and ultra-high MRI imaging studies show that the AD pathology, the diffusion pattern of intra-neuronal neurofibrillary tangles (NFTs), causes selective neurodegeneration on hippocampal subfields (Braak and Braak, 1991, 1997b; Fukutani et al., 2000b; Lace et al., 2009; Schonheit et al., 2004), and consequently leads to macroscopical complex atrophy on hippocampus. Increasing histological and 7T studies show sensitivity on the AD spectrum, supporting the hypothesis that the hippocampal atrophy is a continuous and dynamic process in AD continuum (McKiernan and O'Brien, 2017). One of the current major problems in AD interventions is to find early AD-affected local hippocampal atrophy patterns, so as to incorporate them into early structural biomarkers for AD pre-diagnosis and prognosis. In AD preclinical stage, as one of the earliest targets of neurofibrillary tangle (NFT), Cornu Ammonis (CA1) (specifically the CA1 stratum radiatum) is reported selectively thinning in most histological and 7T MRI studies (Braak and Braak, 1997a; Braak and Braak, 1997b; Kerchner et al., 2010; Scheff et al., 2007). Macrostructural

studies that subdivide the hippocampus by larger scales show consistency that the atrophy on the anterior suffers more rapid atrophy than the posterior at AD preclinical stage (de Flores et al., 2015). However, to date, the relevant consistent local-specific findings have rarely been used as clinical imaging evidence to detect AD progression. Instead, the most widely used clinical method assessing the hippocampal atrophy, the medial temporal lobe atrophy (MTA) score, though provides more specific morphological information than volumetry, relies heavily on expertise (Kaushik et al., 2021). Currently, there is still a lack of a robust and reliable automated quantification method to comprehensively quantify the focal hippocampal atrophy based on clinical imaging, thus to narrow the gap between histological and clinical imaging findings.

The current hippocampal morphological representations based on structural MRI can be categorized into two main approaches: the subfield-volume-based (Gabere et al., 2020; Zhang et al., 2020) and the surface-based representation (Biffi et al., 2020; Chapleau et al., 2020). The subfield-volume-based methods depend heavily on subfield segmentation accuracy, and do not provide sufficient descriptions of local atrophy. Therefore, many studies turn to the surface-based methods, which capture more subtle morphological variations than the volume-based methods. To discover more consistent disease-specific atrophy patterns on clinical imaging, the local atrophy of the macrostructure of the hippocampal shape, instead of the individual subfields, is investigated in these studies (Biffi et al., 2020; Chapleau et al., 2020; Gerardin et al., 2009; Shi et al., 2013; Tang et al., 2015). The main problem of the surface-based methods is that they indirectly describe the hippocampal atrophy by surface changes, whereas the

"atrophy" is actually a morphological change on a three-dimensional anatomy. This problem leads to that the measurements derived from surface-based methods are inadequately interpretable in clinical settings and incomparable with histological findings. The relevant measurements are such as surface area contractions (Das et al., 2012; Tang et al., 2015), curvature changes (Shi et al., 2013), etc. Histologically, the process of the hippocampal atrophy is characterized by anisotropic decrease of local thickness, width and length on hippocampus (McKiernan and O'Brien, 2017), which can be hardly described by the surface-based representations. The 3D hippocampus is a bending archicortex with obvious folds on its head (DeKraker et al., 2021). For such a single anatomical structure, the existed algorithms measuring thickness (Adler et al., 2018; Masouleh et al., 2020) for 3D cortex cannot be directly transplanted into the hippocampus (Jones et al., 2000). It is also difficult to describe the hippocampal atrophy through radial atrophy thickness (Moon et al., 2018), because the thickness measuring lines may intersect with incorrect counterpart points due to the fold on head of hippocampus. These problems lead to inaccurate detection of local atrophy patterns. Further, it is a challenge to detect subtle shape variations across AD development, compared with larger inter-individual differences. The commonly used registration-based methods are difficult to establish stable morphological correspondence between individuals (DeKraker et al., 2021). Overall, due to the complexity of the hippocampal structure and its atrophy, it is necessary to develop a more comprehensive and precise representation to describe the hippocampal morphology.

To map histological distinctive features onto MR images and identify unique local hippocampal atrophy patterns of MCI-to-AD converters during the prodromal stage of AD, we collect longitudinal MRI data from the Alzheimer's Disease Neuroimaging Initiative (ADNI) database, including amyloid-β positive progressive Mild Cognitive Impairment (pMCI) patients, amyloid-β positive stable Mild Cognitive Impairment (sMCI) patients and amyloid-β negative cognitive normal subjects (CN) with 3 scans for 1 year intermittent. To comprehensively describe the hippocampal morphological changes during AD progression, we model the hippocampal shape by a multiscale skeletal representation (m-s-rep). The m-s-rep is developed based on skeletal representation (s-rep), which captures rich 3D intrinsic geometric properties of an object and is statistically stable (Liu et al., 2021; Pizer et al., 2020; Siddiqi et al., 2008; Tu et al., 2018). We develop the method by s-rep interpolating and surface sub-regional atlas projection, so as to assess the large-to-small scale hippocampal morphological variations during AD progression. Different from the surface-based methods, the measurements derived from our representation are more clinically interpretable. To precisely characterize temporal properties of the atrophy patterns related to each experiment group, we improve the intra-subject morphological correspondence by aligning the m-s-reps through a surface-based deformation field from the baseline hippocampus to the hippocampi at other time points. We evaluate AD-sensitivity of the measurements derived from the hippocampal shape representations by group-wise hypothesis tests. The results show remarkable consistency between histological and MRI findings, and spatiotemporal anisotropic atrophy of the hippocampus under the effect of AD. The results also indicate distinctive hippocampal atrophy trajectories between the pMCI and sMCI patients.

2 *Materials and Methods*

We aim to evaluate local atrophy of the hippocampus related to the Aβ positive pMCI and sMCI progression. For this purpose, we collect longitudinal data of pMCI, sMCI and cognitive normal controls from an open-source database, detailed in section 2.1. The data is segmented and extracted hippocampi (section 2.2). The hippocampi are represented by a multiscale skeletal representation method. Cross-sectional/longitudinal measurements are extracted based on the shape representation (section2.3). The statistical analysis is described in section 2.4. Our analysis pipeline is outlined in Figure 1, to give a whole picture of our methods in this study.

2.1 Datasets

Data used in preparation of this study is obtained from the opensource Alzheimer's Disease Neuroimaging Initiative (ADNI) database (http://adni.loni.usc.edu) with three 3T MRI T1-w scans for one year intermittent. All participants have provided informed written consent before recruitment and filled out questionnaires approved by the respective Institutional Review Board (IRB). A subject is labeled as amyloid-β positive based on CSF Aβ1-42 measurement (<192 pg/ml) (Landau et al., 2013; Shaw et al., 2009). Only the pMCI subjects who diagnosed as AD at their third visits and have positive status of CSF Aβ measurement at baseline are selected. The collected CN and sMCI subjects are age and gender matched with pMCI group. The selected CN and sMCI patients remain CSF Aβ negative and positive respectively through all the three visits. All enrolled sMCI and CN subjects keep the same diagnosis through all visits.

According to above criteria, a total of 236 subjects are involved in this study, including 81 CN controls, 88 sMCI and 67 pMCI patients. The demographic information of their baseline examination is presented in table 1.

2.2 Data preprocessing

We deliver the hippocampal segmentation in a pipeline based on a 3D convolutional neural network. The method (called the HippMapp3r) has been proved outperformed some other approaches in AD and elderly population (Zeng et al., 2020). We test this method in longitudinal segmentation task, showing good performance in whole hippocampal volume and shapes. Each segmentation result is visually examined.

Global normalization is performed to rotationally align all the hippocampi and eliminate individual difference of global sizes. Because our aim is to evaluate the shape variations of hippocampus, no nonlinear deformation is introduced into the preprocessing. The global normalization into common space is via an image registration strategy, illustrated in Figure 1b. First, each longitudinal hippocampus of a subject is registered into the baseline by a boundary-based linear registration of the flirt algorithm (Jenkinson M et al., 2002) in FSL (Greve and Fischl, 2009). Second, all baseline hippocampi are linearly registered into a template hippocampus, which is calculated by averaging all baseline hippocampal shapes using the ANTs toolkit (Avants et al., 2008). Finally, the longitudinal hippocampi at each time points are aligned again into their baseline hippocampi.

2.3 Hippocampus modelling on longitudinal data

2.3.1 The multiscale skeletal representation (m-s-rep) of the hippocampus

By considering the atrophy of the hippocampus as volume loss of a three-dimensional anatomy, we initially represent the hippocampus based on the skeletal representation (s-rep). The s-rep provides a continuous interior-filling skeletal model of an object, which is formed by a set of spoke vectors (p, S) with tail at p and tip at p + S, where p represents points located within the object and S represents the corresponding spoke vectors for p. The union of these spoke vectors forms the interior of the object, while the union of their tips forms the object's boundary. The tails of the spoke vectors, which form a folded double-sided surface, are called the skeletal locus. Mathematically, none of the spokes should intersect with each other. In this conventional view, each smooth point p is associated with two spokes, called the up and down spokes, respectively. The spokes attached to fold points of the skeletal locus are called the crest spokes. A typical hippocampus is fitted by the s-rep shown in the left panel of Figure 2. A detailed description of s-rep theory can be found in (Pizer et al., 2020).

The initial s-reps of the hippocampi are generated using an automated method described in (Liu et al., 2021). To balance the computational burden and representation accuracy, we select appropriate parameters for the s-rep models, which are described in detail in the Supplementary Material 1. From the s-rep data, we are able to represent the shape of the hippocampus by spokes. By continuously connecting the spoke tips, we get the implied surface of the hippocampus. As shown in Figure 2, a yellow area is filled with spokes and bounded by the implied surface. However, the implied surface of the initial s-rep cannot precisely match the boundary surface of the hippocampus. Therefore, we adjust the lengths of the spokes to

precisely meet the boundary surface of the hippocampus. In addition, the crest spoke attached on the tip of the skeleton locus may not always point to the tip of the hippocampus, which can result in incorrect locations for atrophy on hippocampal tails (an example is shown in the left panel of Figure 2). This incorrect location may lead to wrong measurement of length and long-axis curvature of the hippocampal shape. Therefore, we compulsorily position the tip crest spoke to the tip of the hippocampal tail. The tip of the hippocampal tail is defined as the point which has highest mean curvature on the surface of the hippocampal tail.

While the initial s-rep model can represent general shape of the hippocampus, it can neither capture subfields nor detailed local characterizations. To comprehensively evaluate the hippocampal atrophy during the disease progression, interpolation for original s-reps to cover all vertices on the hippocampal surface is implemented. Based on this interpolated s-rep, we propose a multiscale skeletal representation (m-s-rep). The “multiscale” refers to the ability to represent the morphology of the hippocampus at different scales, so as to quantify its morphological features from a global to a local scale. The multiscale measurement method covers four scales that encompass 1) the global shape, 2) the tripartite partition (head, body and tail), 3) the subfields on each partition and 4) the detailed local thickness with respect to each point on the surface.s

A s-rep refinement method (Liu et al., 2021) is used to calculate the interpolated s-reps, which takes into account both surface fitness and s-rep geometry. A total of 1738 spokes are calculated to represent each individual hippocampus, with each vertex having a corresponding spoke in its neighborhood. Additionally, the interpolated spokes are fitted to the original hippocampal

surface to better characterize delicate local morphology. An example of the interpolated crest spokes of a hippocampus is shown in the right panel of Figure 1c. To realize regional analysis on the hippocampus, we project a hippocampal subfield atlas onto the spokes of the hippocampus. Specifically, we use an averaged histological and 7T MRI-derived atlas (Adler et al., 2018) as a template and project the subfields on the surface onto each implied surface of the hippocampus by point-wise surface correspondence built by the SPHARM-PDM (spherical harmonic description point distribution models) (Styner M et al., 2006). Then, each spoke tip is assigned to the subfield label according to its nearest point on the implied surface. Subfield labels on the boundary surface are mapped to the skeletal locus through spokes, as shown in Figure 1c. By projecting subfields onto the spokes, we can group the spokes by regions, then generate regional measurements from these spokes.

2.3.2 Improving correspondence on longitudinal data

The determination of point-wise correspondence across objects is a key subject in morphological analysis. The s-rep model provides intrinsic geometric features that allow for cross-sectional correspondence to be established through transformations from ellipses (Liu et al., 2021). However, the cross-sectional correspondence is insufficient for intra-subject analysis. To enhance the longitudinal correspondence, we propose a strategy that deform the baseline s-rep to fit hippocampi observed on other time points. Our basic assumption is that individual hippocampi undergo relatively small variations over time, and their anatomical surface remains smooth. This is typically the case in the prodromal stage of Alzheimer's disease, during which the hippocampi experience minor variations. Firstly, we build surface correspondence among

intra individuals by the SPHARM-PDM method. We set dense control points on each vertex of the surface mesh, and use the thin-plate spline (TPS) method to smoothly transform the baseline surface and its s-rep to fit the hippocampal surfaces on other time points. The deformed s-reps are then refined to better fit the surface boundaries and maintain the s-rep geometry. This process is illustrated in Figure 1d.

2.3.3 Measurement of the hippocampal morphology

The global shape of a hippocampus is represented by a m-s-rep, composed of spoke locations, directions and lengths. While the features derived from m-s-reps are intrinsic geometric features for hippocampal morphology, they are not easily understandable in clinical settings. To improve the interpretability, we define new measurements based on the m-s-rep. Specifically, we measure the hippocampal morphology in terms of length (anterior-posterior extent), width (lateral-medial extent), thickness, and curvature of the long-axis (anterior-posterior axis). Regional-specific thickness and width are calculated by averaging the measurements for each region. The definitions for these measurements are provided in detail below.

The hippocampal long-axis can be represented by the central line of the skeletal locus. To determine the length of the whole hippocampus, we measure the length of the long-axis and add the lengths of two crest spokes attached at the end of the long axis. A length measuring line is shown in orange in the top panel of Figure 1 (e). Similarly, we define the width of the hippocampus by measuring the width of the skeletal sheet and adding the lengths of the

corresponding two crest spokes on tips of the width measuring lines. The blue lines in the top panel of Figure 1 (e) illustrate this measurement.

The thickness and width of the subfield/tripartition of the hippocampus are calculated by grouping same labels of spokes and calculating means of thickness/width on each label. The thickness between the superior and the inferior surfaces involves two subfield labels. We represent the regional thickness by "the subfield label on the superior + the subfield label on the superior", for example, the "CA1 + SUB".

The local thickness at each vertex on the superior hippocampal surface is defined as the length of its corresponding up spoke. Similarly, the local thickness measured on the inferior hippocampal surface is defined as the lengths of the down spokes. The thicknesses between the superior and the inferior surfaces are determined by summing of lengths of the up and down spokes, as illustrated in the middle panel of Figure 1(e). This definition of thickness is robust for two reasons: (1) it assigns a thickness value to every point on the boundary; (2) each point on the surface has a unique thickness value and (3) there is no ambiguity in the measurement of thickness at the hippocampal fold, as the measuring lines start from one side of the surface do not intersect with incorrect points on the counterpart side of surface. Additionally, this definition can be seen as a reasonable simplification of the thickness defined by Laplace's equation, as previously described by (Jones et al., 2000; Tustison et al., 2014).

The long-axis curvature is determined by the curvature of a discrete curve on the skeletal locus surface (Renka, 2005). The bottom panel of Figure 1 (e) shows an example of long-axis of the

hippocampus based on m-s-rep. The bending (curvature increase) or straightening (curvature decrease) of the long-axis is a consequence of anisotropic atrophy of the hippocampal shape. Since previous research (Adler et al., 2018) has identified this feature as a significant difference in hippocampal morphologies between individuals with Alzheimer's disease (AD) and normal controls, we consider the long-axis curvature to be a potentially useful measurement for hippocampal atrophy quantification.

2.3.4 Longitudinal measurements for hippocampal atrophy

To evaluate temporal variations, we define longitudinal measurements by the annualized change rate (ACR) of above cross-sectional measurements (thickness, width, long-axis curvature). The ACR of each cross-sectional measurement is defined as the slope of linear regression of all longitudinal mean measurements vs. scan date differences from baseline (Xie et al., 2020a). Note that to correct for individual differences in head size, we divide the absolute hippocampal volume by the intracranial volume.

2.4 Statistical analysis

We test the between-group difference of the global shape measurement using a specific strategy. Note that s-rep data are defined on a product of Euclidean and non-Euclidean spaces, where the spoke lengths are real numbers that live in the Euclidean space and the spoke positions and directions are in the three-dimensional spherical space (Pizer et al., 2020). Therefore, the geometric elements of spokes exist in the non-Euclidean space and are spatially correlated. This poses a critical challenge for statistically analyzing measurements derived from the skeletal

model. To address these issues, we adopt a permutation test tailored for the s-rep features proposed by (Schulz et al., 2016) to test global shape difference between groups. To be specific, we first calculate the means for a group of hippocampal s-reps by the composite principal nested sphere (CPNS) method (Pizer et al., 2020), which has been proved with superior performance in dealing with s-rep data. In CPNS, the abstract space of the s-rep data is separated into several spheres and real spaces. The real variables are representing spoke lengths and shape sizes so that they are all positive. These variables are log-transformed and rescaled so that they are commensurate with each other, and then calculated arithmetic means. The analysis of the spherical parts begins with the data on a high dimensional sphere, then iteratively fit a lower dimensional subspheres by an analytical computation of means (Pizer et al., 2013). The group means difference concerning both Euclidean and non-Euclidean components is constructed (the difference between spoke directions are measured by longitude and latitude differences). To account for the multivariate nature of the s-rep elements, these differences are mapped to a standard normal distribution, and the covariance matrix is estimated. Next, based on the cutoff value for the empirical distribution of the Mahalanobis distance, a global test is performed to identify global shape differences between groups. Individual features tests are conducted based on a single multivariate test with appropriate FWER inferences. Details of the method can be found in (Schulz et al., 2016). The statistical analysis code by CPNS non-Euclidean hypothesis test is uploaded on XXX.

We test the volume, reginal and local scale measurements, including volume, length, thickness, width, long-axis curvature, local thickness, and the longitudinal measurements using general

linear models. Each measurement is set as the dependent variable, group membership as the factor of interest, and age as covariate. Sex was included as an additional covariate for cross-sectional volume measurements. FDR correction for multiple comparisons is performed (Benjamini and Yekutieli, 2001). Cohen's d is used as a measure of effect size (d), which can be considered as small (0.2), medium (0.5), or large (0.8) effect sizes.

3 Results

The statistical analysis results for group comparisons are summarized in Table 2 and Figure 3~6. Results in Table 2 shows between-group global shape difference tested by the CPNS non-Euclidean hypothesis test method. Results in Figure 3 and 5 are cross-sectional and longitudinal volume and regional measurements tested using the general linear models in the left and right hippocampus respectively. Results in Figure 4 and 6 are cross-sectional and longitudinal local thickness also tested by the general linear models. The descriptions of the results are in details below.

3.1 Difference between the pMCI progression and aging on cross-sectional measurements

Left hippocampus

As shown Table 2, we find significant global shape difference between the pMCI and CN group, and an increasing in the global shape difference from t0 to t2. In Figure 3, the effect size using Cohen's d is shown as color bar, and the p value < 0.05 is marked by star. As shown in Figure

3Aa, the left hippocampus of pMCI group has significant less volume than the CN controls at all time points ($p_{t0}<0.001$, $d_{t0}=1.30$; $p_{t1}<0.001$, $d_{t1}=1.38$; $p_{t2}<0.001$, $d_{t2}=1.43$).

When tripartite the hippocampus into head, body, and tail, we observe that the pMCI group has significant less lateral-medial width in head ($p_0<0.001$, $d_{t0}=0.89$; $p_{t1}<0.001$, $d_{t1}=0.91$; $p_{t2}<0.001$, $D_{t2}=1.01$) body ($p_{t0}<0.001$, $d_{t0}=0.89$; $p_{t1}<0.001$, $d_{t1}=0.98$; $p_{t2}<0.001$, $d_{t2}=1.00$) and tail ($p_{t0}<0.001$, $d_{t0}=0.85$; $p_{t1}<0.001$, $d_{t1}=0.88$; $p_{t2}<0.001$, $d_{t2}=0.96$) parts than the CN controls at all time points. As is shown in Figure 3Ac, in two years preceding to conversion, the means of width for the pMCI group (head: 17.17±1.80mm, body: 14.24±1.67mm, tail: 15.40±1.94mm) has around 1.8mm less than those of the CN group (head: 18.96±1.83mm, body: 15.95± 1.75mm, tail: 17.24±1.97mm).

We further investigate difference in the subfield relevant regional thickness. The measurements that have significant group different between the pMCI and CN groups through all time points including thickness in CA1+SUB ($p_{t0}=0.045$, $d_{t0}=0.36$; $p_{t1}=0.002$, $dt_1=0.53$; $p_{t2}<0.001$, $d_{t2}=0.61$) and CA1+CA1 in the head ($p_{t0}<0.001$, $d_{t0}=0.64$; $p_{t1}<0.001$, $d_{t1}=0.69$; $p_{t2}<0.001$, $d_{t2}=0.73$), CA1+CA1 in the body ($p_{t0}<0.001$, $d_{t0}=0.89$; $p_{t1}<0.001$, $d_{t1}=1.00$; $p_{t2}<0.001$, $d_{t2}=0.97$) and DG+SUB ($p_{t0}=0.038$, $d_{t0}=0.42$; $p_{t1}=0.002$, $d_{t1}=0.58$; $p_{t2}=0.002$, $d_2=0.53$) in the tail.

The first row of the Figure 4A presents results for local thickness comparisons for the pMCI and CN groups at each time point. The largest effect size is 1.17 in the lateral part of the body (CA1+CA1 region). The means difference is 1.17mm ($M_{pMCI}=10.69$mm, $SD_{pMCI}=2.00$mm; $M_{CN}=11.86$mm, $SD_{CN}=2.12$mm).

Right hippocampus

As shown in Table 2, we find significant global shape difference between the pMCI and CN group. In Figure 5Aa, the right hippocampus of the pMCI group has significant less volume than the CN controls at all time points (p_{t0}<0.001, d_{t0}=1.36; p_{t1}<0.001, d_{t1}=1.41; p_{t2}<0.001, d_{t2}=1.48), with effect size increases across time points.

Regarding the measurements in hippocampal head, body, and tail, we show in Figure 5Aa that the pMCI group has significant less lateral-medial width in head (p_{t0}<0.001, d_{t0}=0.91; p_{t1}<0.001, d_{t1}=0.96; p_{t2}<0.001, d_{t2}=1.00), body (p_{t0}<0.001, d_{t0}=0.98; p_{t1}<0.001, d_{t1}=1.02; p_{t2}<0.001, d_{t2}=1.11) and tail (p_{t0}<0.001, d_{t0}=0.87; p_{t1}<0.001, d_{t1}=0.87; p_{t2}<0.001, d_{t2}=0.99) than the CN controls at all time points, with effect size increases across time points. From Figure 3Ac, we observe that the means of lateral-medial width for the pMCI group (head: 18.29±1.54mm, body: 14.57±1.64mm, tail: 16.55±1.92mm) has around 1.8mm less than those of the CN group (head: 20.03±1.82mm, body: 16.39±1.61mm, tail: 18.43±1.99mm) in two years before AD conversion. Moreover, the pMCI group has less thickness in head (p_{t0}<0.001, d_{t0}=0.58; p_{t1}<0.001, d_{t1}=0.65; p_{t2}<0.001, d_{t2}=0.74), body (p_{t0}<0.001, d_{t0}=0.58; p_{t1}<0.001, d_{t1}=0.64; p_{t2}<0.001, d_{t2}=0.74) and posterior (p_{t0}=0.004, d_{t0}=0.55; p_{t1}=0.002, d_{t1}=0.48; p_{t2}<0.001, d_{t2}=0.60) than the CN group.

Measurements in regions of hippocampal head that are significant less than those of the CN group includes thickness in SUB+SUB (p_{t0}=0.003, d_{t0}=0.47; p_{t1}=0.003, d_{t1}=0.46; p_{t2}=0.001, d_{t2}=0.58), CA1+SUB (p_{t0}=0.045, d_{t0}=0.67; p_{t1}=0.002, d_{t1}=0.75; p_{t2}<0.001, d_{t2}=0.80), CA1+CA1 (p_{t0}<0.001, d_{t0}=0.63; p_{t1}<0.001, d_{t1}=0.68; p_{t2}<0.001, d_{t2}=0.68), CA2+SUB (p_{t0}<0.001, d_{t0}=0.66; p_{t1}<0.001, d_{t1}=0.69; p_{t2}<0.001, d_{t2}=0.68), CA3+DG (p_{t0}=0.001, d_{t0}=0.53; p_{t1}<0.001, d_{t1}=0.59;

p_{t2}<0.001, d_{t2}=0.66) and SRLM+CA1 (p_{t0}<0.001, d_{t0}=0.59; p_{t1}<0.001, d_{t1}=0.73; p_{t2}<0.001, d_{t2}=0.83). Significant difference are also found in thickness of several regions in hippocampal body, including the CA1+CA1(p_{t0}<0.001, d_{t0}=0.91; p_{t1}<0.001, d_{t1}=0.92; p_{t2}<0.001, d_{t2}=1.10), CA2+CA1 (p_{t0}=0.013, d_{t0}=0.42; p_{t1}=0.007, d_{t1}=0.46; p_{t2}<0.001, d_{t2}=0.58), CA3+SUB (p_{t0}=0.005, d_{t0}=0.49; p_{t1}=0.004, d_{t1}=0.50; p_{t2}<0.001, d_{t2}=0.59) and CA3+CA3 (p_{t0}=0.053, d_{t0}=0.49; p_{t1}=0.039, d_{t1}=0.35; p_{t2}=0.009, d_{t2}=0.42). Thickness in the CA1+CA1 of the hippocampal tail of the pMCI group is less than that of the CN group (p_{t0}=0.002, d_{t0}=0.49; p_{t1}=0.002, d_{t1}=0.50; p_{t2}<0.001, d_{t2}=0.55). In two years preceding to AD conversion, the two groups have largest means difference of 0.70mm in CA3+CA3 region in the body (M_{pMCI}=4.45mm, SD_{pMCI}=1.99mm; M_{CN}=5.15mm, SD_{CN}=2.11mm).

The first row of the Figure 6A presents results for local thickness comparisons of the pMCI and CN groups at each time point. Two years before conversion, the largest effect size is 1.15 in the CA3+CA3 region in medial part of the body. The means difference is 1.47mm (M_{pMCI}=12.20mm, SD_{pMCI}=2.15mm; M_{CN}=13.66mm, SD_{CN}=2.18mm).

3.2 Difference between the sMCI progression and aging on cross-sectional measurements

Left hippocampus

The sMCI group has significant global shape difference from the CN group, and an increasing of test statistics are shown in Table 2. Figure 3Ab presents the group comparison results for global and regional measurements at three time points between sMCI and CN groups. Less significant differences are discovered for the sMCI group than the pMCI group when compared

with CN controls. The sMCI group has less hippocampal volume than the CN group at all time points (p_{t0}<0.001, d_{t0}=0.79; p_{t1}<0.001, d_{t1}=0.81; p_{t2}<0.001, d_{t2}=0.84).

As in shown in Figure 3Ab the sMCI group has significant less lateral-medial width in head (p_{t0}<0.001, d_{t0}=0.61; p_{t1}<0.001, d_{t1}=0.59; p_{t2}<0.001, $_{t2}$=0.66) body (p_{t0}<0.001, d_{t0}=0.62; p_{t1}<0.001, d_{t1}=0.61; p_{t2}<0.001, d_{t2}=0.61) and tail (p_{t0}=0.001, d_{t0}=0.57; p_{t1}<0.001, d_{t1}=0.61; p_{t2}<0.001, d_{t2}=0.61) than the CN controls at all time points.

The second row of the Figure 4A presents results for local thickness comparisons of the sMCI and CN groups at each time point. No local measurement has significant difference at all three time points. The lateral of body and the tail tip show significant difference at the second time point.

Right hippocampus

As show in Table 2, the sMCI and CN groups have significant global shape difference. Figure 5Ab presents the group comparison results for global and regional measurements at three time points between sMCI and CN groups. The right hippocampi of sMCI group have less volume than that of the CN group at all time points (p_{t0}<0.001, d_{t0}=0.88; p_{t1}<0.001, d_{t1}=0.88; p_{t2}<0.001, d_{t2}=0.92).

As shown in Figure 3Ab, the sMCI group has significant less lateral-meidal width of head (p_{t0}<0.001, d_{t0}=0.63; p_{t1}<0.001, d_{t1}=0.63; p_{t2}<0.001, d_{t2}=0.63), body (p_{t0}<0.001, d_{t0}=0.70; p_{t1}<0.001, d_{t1}=0.70; p_{t2}<0.001, d_{t2}=0.71) and tail (p_{t0}<0.001, d_{t0}=0.66; p_{t1}<0.001, d_{t1}=0.64; p_{t2}<0.001, d_{t2}=0.63) than the CN controls at all time points.

3.3 Difference between the pMCI and sMCI progression on cross-sectional measurements

Left hippocampus

The pMCI group has significant difference in the global shape measurement compared with the sMCI group at the last two time points. Figure 3Ac shows that the two groups have already shown significant difference in volume two years prior to conversion ($p_{t0}<0.001$, $d_{t0}=0.58$; $p_{t1}<0.001$, $d_{t1}=0.67$; $p_{t2}<0.001$, $d_{t2}=0.73$).

Among regional measurements, only the thickness of CA1+CA1 in the body has significant group difference between the pMCI ($M_{t0}=6.47$mm, $SD_{t0}=0.47$mm) and sMCI group ($M_{t0}=6.72$mm, $SD_{t0}=0.49$mm) through all time points ($p_{t0}=0.017$, $d_{t0}=0.52$; $p_{t1}=0.004$, $d_{t1}=0.57$; $p_{t2}=0.002$, $d_{t2}=0.58$).

The third row of the Figure 4A presents results for local thickness comparisons between the sMCI and pMCI groups at each time point. Although we observe locations that have significant difference in two years before AD conversion (mainly in the CA1+CA1 region in the body), measurements at these locations are absent of significant difference at following time points. The medial part of body and the top of anterior show significant difference in the last year before AD conversion, where the largest means difference is 1.21mm (p=0.012, d=0.595, $M_{pMCI}=10.31$mm, $SD_{pMCI}=1.67$mm; $M_{sMCI}=11.5$mm, $SD_{sMCI}=2.13$mm) in SRLM+CA1.

Right hippocampus

The pMCI group has significant difference in the global shape measurement compared with the sMCI group at all time points. Figure 5Ac shows that the right hippocampal volume of pMCI group is significant less than that of the CN group at all time points (p_{t0}<0.001, d_{t0}=0.60; p_{t1}<0.001, d_{t1}=0.67; p_{t2}<0.001, d_{t2}=0.76).

The pMCI group has significant less thickness in head (p_{t0}=0.002, d_{t0}=0.52; p_{t1}<0.001, d_{t1}=0.59; p_{t2}<0.001, d_{t2}=0.61) and body (p_{t0}=0.001, d_{t0}=0.59; p_{t1}<0.001, d_{t1}=0.64; p_{t2}<0.001, d_{t2}=0.68) than the sMCI group. The pMCI group also has significant less thickness in the posterior (p_{t0}=0.003, d_{t0}=0.50; p_{t1}=0.002, d_{t1}=0.54; p_{t2}=0.003, d_{t2}=0.51) than that of the sMCI controls at all time points.

Thickness in hippocampal head including SUB+SUB (p_{t0}=0.010, d_{t0}=0.45; p_{t1}=0.005, d_{t1}=0.48; p_{t2}=0.002, d_{t2}=0.50), CA1+SUB (p_{t0}=0.002, d_{t0}=0.53; p_{t1}<0.001, d_{t1}=0.61; p_{t2}<0.001, d_{t2}=0.64), CA1+CA1 (p_{t0}=0.003, d_{t0}=0.52; p_{t1}=0.005, d_{t1}=0.47; p_{t2}<0.001, d_{t2}=0.62), CA2+SUB (p_{t0}=0.002, d_{t0}=0.52; p_{t1}=0.001, d_{t1}=0.54; p_{t2}<0.001, d_{t2}=0.59), CA3+DG (p_{t0}=0.010, d_{t0}=0.44; p_{t1}=0.007, d_{t1}=0.45; p_{t2}<0.001, d_{t2}=0.62), SRLM+CA1 (p_{t0}=0.002, d_{t0}=0.57; p_{t1}<0.001, d_{t1}=0.64; p_{t2}<0.001, d_{t2}=0.67) of the pMCI group are less than those of the CN group. Thickness of regions in hippocampal body, including the CA1+CA1(p_{t0}<0.001, d_{t0}=0.64; p_{t1}<0.001, d_{t1}=0.70; p_{t2}<0.001, d_{t2}=0.78), CA3+SUB (p_{t0}=0.002, d_{t0}=0.54; p_{t1}=0.002, d_{t1}=0.55; p_{t2}<0.001, d_{t2}=0.59) and CA3+CA3 (p_{t0}=0.013, d_{t0}=0.44; p_{t1}=0.031, d_{t1}=0.38; p_{t2}=0.002, d_{t2}=0.52) of the pMCI group, are less than those of the CN group.

The third row of the Figure 6A presents results for local thickness comparisons between the sMCI and pMCI groups at each time point. We observe that the pMCI group has less thickness

of the body and medial head than the sMCI group in two years before conversion. Atrophy locations spread to whole part of the head at following time points. In two years before conversion, the two groups have largest means difference of local thickness 0.80mm ($p=0.004$, $d=0.52$, $M_{pMCI}=6.05$mm, $SD_{pMCI}=1.12$mm; $M_{sMCI}=6.85$mm, $SD_{sMCI}=1.59$mm) in the medial of the body (CA3+CA3).

3.4 Between-group differences on Longitudinal measurements

Left hippocampus

As shown in Figure 3Ba, the pMCI group has significant less volume decreasing rate than CN and sMCI groups ($p_{CNvs.pMCI}<0.001$, $d_{CNvs.pMCI}=1.08$; $p_{sMCIvs.pMCI}<0.001$, $d_{CNvs.pMCI}=0.66$). The pMCI group has higher decreasing rate in lateral-medial width of head ($p<0.007$, $d=0.54$) and body ($p<0.043$, $d=0.41$), and thickness of head ($p<0.001$, $d=0.69$) than the CN group. Regarding subfield-relevant regional thickness, regions in SUB+SUB ($p=0.007$, $d=0.53$) and CA1+SUB ($p=0.003$, $d=0.68$), CA2+SUB ($p=0.020$, $d=0.47$), CA3+DG ($p=0.045$, $d=0.41$) and SRLM+CA1 ($p=0.030$, $d=0.44$) in the hippocampal head of the pMCI group has less thickness decreasing rate than the CN group.

Figure 4B shows group comparison results of local thickness decreasing rate. We observe that the pMCI group has widely spread focal atrophy rate than the CN controls, particularly in the middle and lateral part of the hippocampus. Local thickness of pMCI group shows highest decreasing rate of -2.89%/year (SD=5.69%/year) in medial hippocampal head near SRLM, and the thickness change rate of sMCI and CN group in the corresponding location are -0.37%/year

(SD=4.20%/year) and -0.56%/year (SD=3.64%/year) respectively. Additionally, the largest means difference is 3.05%/year (p=0.011, d=0.53, M_{pMCI}=-2.82%/year, SD_{pMCI}=6.45%/year; M_{CN}=0.23%/year, SD_{CN}=4.66%/year) in the medial hippocampal head near SRLM. The sMCI and CN group has no significant differences in local thickness decreasing rate. As shown the last column, significant higher focal atrophy rate of the pMCI than the sMCI has been discovered mainly in a small lateral part of the hippocampus (CA2+CA1 region in the body), while the largest means difference is 2.89%/year (p=0.034, d=0.54, M_{pMCI}=-2.87%/year, SD_{pMCI}=6.04%/year; M_{pMCI}=-0.02%/year, SD_{pMCI}=4.34%/year) found in medial hippocampal head near SRLM.

Right hippocampus

As shown in Figure 5Ba, the pMCI group has significant less volume decreasing rate than CN and sMCI groups ($p_{CNvs.pMCI}$<0.001, $d_{CNvs.pMCI}$=1.11; $p_{sMCIvs.pMCI}$<0.001, $d_{CNvs.pMCI}$=0.71). The pMCI group has higher decreasing rate in lateral-medial width of head ($p_{CNvs.pMCI}$<0.001, $d_{CNvs.pMCI}$=0.68; $p_{sMCIvs.pMCI}$<0.001, $d_{CNvs.pMCI}$=0.60), body ($p_{CNvs.pMCI}$<0.001, $d_{CNvs.pMCI}$=0.73; $p_{sMCIvs.pMCI}$<0.001, $d_{CNvs.pMCI}$=0.62) and tail ($p_{CNvs.pMCI}$<0.001, $d_{CNvs.pMCI}$=0.61; $p_{sMCIvs.pMCI}$<0.001, $d_{CNvs.pMCI}$=0.58) than the CN and sMCI groups. The pMCI group has significant less thickness decreasing rate in head (p=0.002, d=0.55) and body (p=0.013, d=0.49) than the CN group. Regarding subfield-relevant regional thickness, the pMCI group has less thickness decreasing rate than the CN group in several regions in the head including SUB+SUB (p=0.032, d=0.384), CA1+SUB (p=0.004, d=0.513), CA2+SUB (p=0.011, d=0.48) and SRLM+CA1 (p<0.001, d=0.65). The pMCI group also has less thickness decreasing rate in CA1+CA1 (p<0.001,

d=0.73) and CA2+CA1 (p=0.032, d=0.42) regions in the body than the CN group. The pMCI group has significant less thickness compared with sMCI group in CA1+SUB (p=0.040, d=0.42) in the head and CA1+CA1 (p=0.037, d=0.43), CA2+CA1 (p=0.030, d=0.45) regions in the body.

Figure 6B shows group comparison results of local thickness decreasing rate. We observe that the pMCI group has focal atrophy rate than the CN controls in the middle and medial part of the hippocampus. Local thickness of pMCI group shows highest decreasing rate of -2.96%/year (SD=5.70%/year) in the medial hippocampal head near SRLM, and the thickness change rate of sMCI and CN group in the corresponding location are 0.40%/year (SD=7.79%/year) and -0.87%/year (SD=5.56%/year) respectively. Additionally, the largest means difference is 2.64%/year (p=0.021, d=0.47, M_{pMCI}=-2.38%/year, SD_{pMCI}=6.12%/year; M_{CN}=0.26%/year, SD_{CN}=4.79%/year) in the medial hippocampal head near SRLM. The sMCI has no significant differences in local thickness decreasing rate compared with CN and pMCI groups.

4 Discussion

We propose a shape model to evaluate local hippocampal atrophy during prodromal AD based on 3T T1-w images. This shape model enables a large-to-small scale description of the spatiotemporal morphological changes in the hippocampus. We implement the method on longitudinal cohorts collected from the ADNI database, including Amyloid-β positive pMCI and sMCI patients, as well as Amyloid-β negative cognitive normal subjects with 3 scans for 1 year intermittent to evaluate cross-sectional and longitudinal hippocampal atrophy during the

MCI progression. The main findings including that: 1) The main hippocampal atrophy of pMCI is dominated by lateral-medial width decrease (approximately 1.8mm less than normal individuals in the two years preceding conversion). The largest difference in local thickness decreasing rates (left: 3.05%/year; right: 2.64%/year) is observed in the medial head of hippocampi. The lateral head of the left hippocampus (SRLM+CA1) experiences thickness decrease of 1.21mm in compared to controls two years before conversion. 2) In the two years preceding conversion, the right hippocampus exhibits more severe and widespread atrophy, including the thickness of certain regions in the head and body, with the largest difference of 0.8mm in the CA3+CA3 region of body in two years preceding to conversion. The local thickness decreasing rate shows the highest difference of 2.89%/year in the medial head of the left hippocampi between pMCI and sMCI.

4.1 The evaluation of hippocampal atrophy in 3T in-vivo MRI obtains consistent findings with MRI and histology studies

In this study, the observed annualized volume decreasing rate of normal aging is 1.09%/year, comparable with that reported in a systematic review in (Fraser et al., 2015) (1.12% for ≥70 years old healthy adults). We observe 2.93%/year and 3.02%/year volume decrease in left and right hippocampus for pMCI; the volume decrease of sMCI are 1.55%/year and 1.56%/year, and the CN are 0.85%/year and 0.84%/year for the left and right side of hippocampi. The results are comparable with those reported MCI volumetric atrophy rate, ranging from 1.55%/year to 3.2%/year in 12 studies (Chincarini et al., 2016; Das et al., 2012; Holland et al., 2012; Iglesias et al., 2016; Jack et al., 2000; Kulason et al., 2019; Ledig et al., 2018; Leung et al., 2010; Morra

et al., 2009; Schuff et al., 2009; Tward et al., 2017; Xie et al., 2020b; Wolz et al., 2010). The difference of the reported atrophy rate in literatures is possibly due to the hippocampal segmentation approaches and different MCI stages included in the experiments.

Our method proposed interpretable measurements for the hippocampal morphology which are comparable to histology findings. In the present study, we observe the hippocampal anterior-posterior extent ("length" in this study) of to be 46.69mm (SD=2.30mm), lower than 50mm reported in histological literatures (Witter et al., 2004), and within the range of an autopsy results (31~51mm) reported in (Adler et al., 2018).

Numbers of studies recognize that the severer anterior atrophy than the posterior is a pattern of AD distinct from normal aging (Adler et al., 2018; Chauveau et al., 2021; Martin et al., 2010). Our experiment shows that the medial-lateral widths (head, body, and tail) of the left and right hippocampi in pMCI are reduced by approximately 1.8mm compared to controls. During the year of pMCI conversion to AD, the thickness of the anterior and posterior regions of the left and right hippocampi is less than CN in bilateral hippocampi, while the anterior thickness difference is larger than the posterior. Specifically, the mean difference in the anterior region of the left hippocampus is 0.42mm (M_{pMCI}=7.97mm, SD_{pMCI}=0.82mm; M_{CN}=8.39mm, SD_{CN}=0.65mm), and in the posterior region is 0.21mm (M_{pMCI}=6.24mm, SD_{pMCI}=0.52mm; M_{CN}=6.45mm, SD_{CN}=0.48mm). The mean difference in the anterior region of the right hippocampus is 0.55mm (M_{pMCI}=7.63mm, SD_{pMCI}=0.83mm; M_{CN}=8.18mm, SD_{CN}=0.55mm), and in the posterior region is 0.30mm (M_{pMCI}=6.17, SD_{pMCI}=0.50; M_{CN}=6.47, SD_{CN}=0.46). Moreover, we test the longitudinal measurements for anterior and posterior difference. The both

sides of the hippocampus of pMCI have higher thickness decreasing rate in anterior than the posterior (p_{left}=0.017, d_{left}=0.46; p_{right}=0.020, d_{right}=0.40), and in the right hippocampus, the lateral-medial width of the posterior decreasing rate is higher than the anterior (p=0.009, d=0.48). The thicknesses of the anterior hippocampus are -1.49%year (SD=2.03%/year) and -1.31/year (SD=1.90%/year) for the left and right side respectively, and the width of the posterior of the right hippocampus decreases -2.28%/year (SD=2.47%/year) and in pMCI. In general, the thickness reduction of the anterior hippocampus in individuals with pMCI is more severe and occurs at a higher decreasing rate, and there is a rapid decrease in the lateral-medial width of the posterior part of the right hippocampus.

For the subfield relevant changes affected by AD, in our results (Figure 3Aa and Figure 5Aa), the pMCI shows an atrophy pattern that most distributed in CA1 and SUB, suggesting a similar diffusing pattern from CA1 and SUB to CA2, CA3 and DG in (Braak and Braak, 1991; Braak et al., 1993; Fukutani et al., 2000a; Kril et al., 2002; Lace et al., 2009; Padurariu et al., 2012; von Gunten et al., 2006). Moreover, in our experiment, the fastest atrophy of the left and right hippocampi occurs in the medial part of the hippocampal head (SRLM+CA1), with an annual rate of 2.89±5.69% for the left side and 2.96±5.70% for the right side. This result is similar with most histological and 7T MRI finding that CA1-SRLM is selectively thinning in early AD (Braak and Braak, 1997a; Braak and Braak, 1997b; Kerchner et al., 2010; Scheff et al., 2007).

4.2 Potential morphometric measures to differentiate Aβ positive pMCI and sMCI in prodromal AD

We find significant less volume of hippocampi for the pMCI than the age-matched sMCI and significant higher volume decreasing rate in pMCI (Left: 2.93±2.14%/year; Right: 3.02±2.09%/year) than that of the sMCI (Left: 1.55±1.85%/year; Right: 1.56±1.76%/year) two years prior to AD conversion. The global shape is also a good measure for group difference comparable with the volume measurement, which shows significant difference in the right hippocampus two years before AD conversion. Analysis on regional and local measurements shows that the pMCI exhibits more severe atrophy on both hippocampal sides than sMCI. Various cross-sectional measurements show differences in two years prior to AD conversion in pMCI rather than sMCI compared with CN. By contrast, the hippocampi of sMCI exhibit significant difference only in the lateral-medial width compared with CN two years prior to AD conversion. In the early stages of Alzheimer's disease (AD), significant differences have been observed between individuals with pMCI and sMCI even before conversion, with the differences spreading from the body to the head of the hippocampus. In the two years preceding conversion, the right hippocampus exhibits more severe and widespread atrophy, affecting the thickness of certain regions in the head and body, including CA1, SUB, and CA3 (Figure 3Ac and Figure 5Ac). The difference between the regional and local thickness of the two groups are almost less than 1mm in two years preceding to conversion. The local thickness in CA3+CA3 region of right hippocampal body has the largest difference of around 0.8mm. While, local thickness analysis results show that the largest difference of 1.21mm occurs in the lateral body of the left hippocampus (SRLM+CA1) in two years prior to AD conversion. In the same region, the local thickness decreasing rate shows the highest difference of 2.89%/year between pMCI and sMCI. These findings indicate distinctive trajectories of atrophy between the two groups,

and the measurements that shows significant difference may be candidate indicators for differentiating the two groups one year prior to AD conversion.

4.3 limitations and future work

Our current study has two main limitations. First, the hippocampal subfield morphology is not investigated in this study considering the low resolution in 3T subfields segmentation and differed segmentation protocols. Second, our statistical analysis method has high requirements for the inclusion criteria of the data (three 3T MRI T1-w scans for one year intermittent), which results in a relatively small sample size. Future directions for this work include the incorporation of subfield morphometric and analysis on large longitudinal samples in order to find useful image markers for early AD detection.

5 Conclusion

In this study, we propose a multiscale skeletal representation (m-s-rep) to characterize the hippocampal shape from a small-to-large scale based on longitudinal 3T T1-w MR images. Based on this method, we investigate hippocampal atrophy patterns associated with the amyloid-β positive pMCI and sMCI. Quantification of local hippocampal atrophy based on 3T T1-w MR images by the proposed method discovers progressive local atrophy pattern that agree with consistent histological and 7T MRI findings. The main hippocampal atrophy of pMCI is dominated by the decreasing of the lateral-medial width of the bilateral hippocampus and a rapid atrophy in medial head. Moreover, the differences between pMCI and sMCI spreading from the body to the head of the hippocampus. In the two years preceding conversion, the right hippocampus exhibits more severe and widespread atrophy in head and body, involving CA1,

SUB and CA3. These results demonstrate that our method can comprehensively evaluate the hippocampal atrophy on clinical data, and provide a potential quantitative tool for the hippocampal morphological evaluation to assist AD pre-diagnosis and prognosis.

Contributors

NG did data cleaning, processing, statistical analyses and drafted the manuscript and figures. ZL assisted the data processing and drafted the manuscript. YD and HC collected and preprocessed the data. CY assisted the experiment design and refined the manuscript. QY supervised data processing. TM conceived and supervised the whole study, and revised the manuscript.

Data availability statement

Data supporting the findings of this study were enrolled from Alzheimer' s Disease Neuroimaging Initiative (ADNI) database: www.loni.ucla.edu/ADNI/. The inclusion and exclusion criteria were listed in "Datasets" section of manuscripts. The corresponding author has full access to the data and codes used in this study, which are available on reasonable request.

Reference

Adler, D.H., Wisse, L.E.M., et al., 2018. Characterizing the human hippocampus in aging and Alzheimer's disease using a computational atlas derived from ex vivo MRI and histology. Proceedings of the National Academy of Sciences of the United States of America 115, 4252-4257.

Avants, B.B., Epstein, C.L., et al., 2008. Symmetric diffeomorphic image registration with cross-correlation: Evaluating automated labeling of elderly and neurodegenerative brain. Medical Image Analysis 12, 26-41.

Barnes, J., Bartlett, J.W., et al., 2009. A meta-analysis of hippocampal atrophy rates in Alzheimer's disease. Neurobiol Aging 30, 1711-1723.

Benjamini Y, Yekutieli D (2001): The control of the false discovery rate in multiple testing under dependency. Ann Stat 29:11651188.

Biffi, C., Cerrolaza, J.J., et al., 2020. Explainable Anatomical Shape Analysis Through Deep Hierarchical Generative Models. Ieee Transactions on Medical Imaging 39, 2088-2099.

Braak, E., Braak, H., 1997a. Alzheimer's disease: transiently developing dendritic changes in pyramidal cells of sector CA1 of the Ammon's horn. Acta Neuropathol 93, 323-325.

Braak, H., Braak, E., 1991. Neuropathological stageing of Alzheimer-related changes. Acta Neuropathol 82, 239-259.

Braak, H., Braak, E., 1997b. Staging of Alzheimer-related cortical destruction. Int Psychogeriatr 9 Suppl 1, 257-261; discussion 269-272.

Braak, H., Braak, E., et al., 1993. Staging of Alzheimer-related cortical destruction. Eur Neurol 33, 403-408.

Chapleau, M., Bedetti, C., et al., 2020. Deformation-based shape analysis of the hippocampus in the semantic variant of primary progressive aphasia and Alzheimer's disease. Neuroimage Clin 27, 102305.

Chauveau, L., Kuhn, E., et al., 2021. Medial Temporal Lobe Subregional Atrophy in Aging and Alzheimer's Disease: A Longitudinal Study. Frontiers in Aging Neuroscience 13.

Chincarini, A., Sensi, F., et al., 2016. Integrating longitudinal information in hippocampal volume measurements for the early detection of Alzheimer's disease. Neuroimage 125, 834-847.

Das, S.R., Avants, B.B., et al., 2012. Measuring longitudinal change in the hippocampal formation from in vivo high-resolution T2-weighted MRI. Neuroimage 60, 1266-1279.

de Flores, R., La Joie, R., et al., 2015. Structural imaging of hippocampal subfields in healthy aging and Alzheimer's disease. Neuroscience 309, 29-50.

DeKraker, J., Kohler, S., et al., 2021. Surface-based hippocampal subfield segmentation. Trends in Neurosciences 44, 856-863.

Dubois, B., Feldman, H.H., et al., 2014. Advancing research diagnostic criteria for Alzheimer's disease: the IWG-2 criteria. Lancet Neurol 13, 614-629.

Fraser, M.A., Shaw, M.E., et al., 2015. A systematic review and meta-analysis of longitudinal hippocampal atrophy in healthy human ageing. Neuroimage 112, 364-374.

Frisoni, G.B., Fox, N.C., et al., 2010. The clinical use of structural MRI in Alzheimer disease. Nature Reviews Neurology 6, 67-77.

Fukutani, Y., Cairns, N.J., et al., 2000a. Neuronal loss and neurofibrillary degeneration in the hippocampal cortex in late-onset sporadic Alzheimer's disease. Psychiatry and Clinical Neurosciences 54, 523-529.

Fukutani, Y., Cairns, N.J., et al., 2000b. Neuronal loss and neurofibrillary degeneration in the hippocampal cortex in late-onset sporadic Alzheimer's disease. Psychiatry Clin Neurosci 54, 523-529.

Gabere, M., Thu Pham, N.T., et al., 2020. Automated Hippocampal Subfield Volumetric Analyses in Atypical Alzheimer's Disease. Journal of Alzheimers Disease 78, 927-937.

Gerardin, E., Chetelat, G., et al., 2009. Multidimensional classification of hippocampal shape features discriminates Alzheimer's disease and mild cognitive impairment from normal aging. Neuroimage 47, 1476-1486.

Greve, D.N., Fischl, B., 2009. Accurate and robust brain image alignment using boundary-based registration. Neuroimage 48, 63-72.

Hill, D.L.G., Schwarz, A.J., et al., 2014. Coalition Against Major Diseases/European Medicines Agency biomarker qualification of hippocampal volume for enrichment of clinical trials in predementia stages of Alzheimer's disease. Alzheimers Dement 10, 421-429 e423.

Holland, D., McEvoy, L.K., et al., 2012. Unbiased comparison of sample size estimates from longitudinal structural measures in ADNI. Human Brain Mapping 33, 2586-2602.

Huang, Y.L., Huang, L., et al., 2022. Differential associations of visual memory with hippocampal subfields in subjective cognitive decline and amnestic mild cognitive impairment. Bmc Geriatrics 22.

Iglesias, J.E., Van Leemput, K., et al., 2016. Bayesian longitudinal segmentation of hippocampal substructures in brain MRI using subject-specific atlases. Neuroimage 141, 542-555.

Jack, C.R., Petersen, R.C., et al., 2000. Rates of hippocampal atrophy correlate with change in clinical status in aging and AD. Neurology 55, 484-489.

Jenkinson M, Bannister P, Brady M, Smith S (2002), Improved optimization for the robust and accurate linear registration and motion correction of brain images. Neuroimage 17:825-841.

Jones, S.E., Buchbinder, B.R., et al., 2000. Three-dimensional mapping of cortical thickness using Laplace's equation. Human Brain Mapping 11, 12-32.

Kaushik, S., Vani, K., et al., 2021. Evaluation of MR Visual Rating Scales in Major Forms of Dementia. Journal of Neurosciences in Rural Practice 12, 16-23.

Kerchner, G.A., Hess, C.P., et al., 2010. Hippocampal CA1 apical neuropil atrophy in mild Alzheimer disease visualized with 7-T MRI. Neurology 75, 1381-1387.

Kril, J.J., Patel, S., et al., 2002. Patients with vascular dementia due to microvascular pathology have significant hippocampal neuronal loss. Journal of Neurology Neurosurgery and Psychiatry 72, 747-751.

Kulason, S., Tward, D.J., et al., 2019. Cortical thickness atrophy in the transentorhinal cortex in mild cognitive impairment. Neuroimage-Clinical 21.

Lace, G., Savva, G.M., et al., 2009. Hippocampal tau pathology is related to neuroanatomical connections: an ageing population-based study. Brain 132, 1324-1334.

Landau, S. M., Lu, M., Joshi, A. D., et al. 2013. Comparing positron emission tomography imaging and cerebrospinal fluid measurements of beta-amyloid. Ann Neurol, 74(6), 826-836.

Ledig, C., Schuh, A., et al., 2018. Structural brain imaging in Alzheimer's disease and mild cognitive impairment: biomarker analysis and shared morphometry database. Scientific Reports 8.

Leung, K.K., Barnes, J., et al., 2010. Automated cross-sectional and longitudinal hippocampal volume measurement in mild cognitive impairment and Alzheimer's disease. Neuroimage 51, 1345-1359.

Liu, Z., Hong, J., et al., 2021. Fitting unbranching skeletal structures to objects. Medical Image Analysis 70, 102020.

Lombardi, G., Crescioli, G., et al., 2020. Structural magnetic resonance imaging for the early diagnosis of dementia due to Alzheimer's disease in people with mild cognitive impairment. Cochrane Database of Systematic Reviews.

Martin, S.B., Smith, C.D., et al., 2010. Evidence that volume of anterior medial temporal lobe is reduced in seniors destined for mild cognitive impairment. Neurobiology of Aging 31, 1099-1106.

Masouleh, S.K., Eickhoff, S.B., et al., 2020. Influence of Processing Pipeline on Cortical Thickness Measurement. Cerebral Cortex 30, 5014-5027.

McKiernan, E.F., O'Brien, J.T., 2017. 7T MRI for neurodegenerative dementias in vivo: a systematic review of the literature. Journal of Neurology Neurosurgery and Psychiatry 88, 564-574.

Moon, S.W., Lee, B., et al., 2018. Changes in the Hippocampal Volume and Shape in Early-Onset Mild Cognitive Impairment. Psychiatry Investig 15, 531-537.

Morra, J.H., Tu, Z., et al., 2009. Automated mapping of hippocampal atrophy in 1-year repeat MRI data from 490 subjects with Alzheimer's disease, mild cognitive impairment, and elderly controls. Neuroimage 45, S3-15.

Padurariu, M., Ciobica, A., et al., 2012. Hippocampal Neuronal Loss in the Ca1 and Ca3 Areas of Alzheimer's Disease Patients. Psychiatria Danubina 24, 152-158.

Renka, R.J., 2005. Shape-preserving interpolation by fair discrete G(3) space curves. Computer Aided Geometric Design 22, 793-809.

Ruchinskas, R., Nguyen, T., et al., 2022. Diagnostic Utility of Hippocampal Volumetric Data in a Memory Disorder Clinic Setting. Cognitive and Behavioral Neurology 35, 66-75.

Scheff, S.W., Price, D.A., et al., 2007. Synaptic alterations in CA1 in mild Alzheimer disease and mild cognitive impairment. Neurology 68, 1501-1508.

Schonheit, B., Zarski, R., et al., 2004. Spatial and temporal relationships between plaques and tangles in Alzheimer-pathology. Neurobiology of Aging 25, 697-711.

Schuff, N., Woerner, N., et al., 2009. MRI of hippocampal volume loss in early Alzheimers disease in relation to ApoE genotype and biomarkers. Brain 132, 1067-1077.

Schulz, J., Pizer, S.M., et al., 2016. Non-linear Hypothesis Testing of Geometric Object Properties of Shapes Applied to Hippocampi. Journal of Mathematical Imaging and Vision 54, 15-34.

Shaw, L. M., Vanderstichele, H., Knapik-Czajka, et al. 2009. Cerebrospinal fluid biomarker signature in Alzheimer's disease neuroimaging initiative subjects. Ann Neurol, 65(4), 403-413.

Shi, F., Liu, B., et al., 2009. Hippocampal Volume and Asymmetry in Mild Cognitive Impairment and Alzheimer's Disease: Meta-Analyses of MRI Studies. Hippocampus 19, 1055-1064.

Shi, J., Thompson, P.M., et al., 2013. Surface fluid registration of conformal representation: Application to detect disease burden and genetic influence on hippocampus. Neuroimage 78, 111-134.

Styner M, Oguz I, Xu S., et al., 2006. Framework for the Statistical Shape Analysis of Brain Structures using SPHARM-PDM. Insight J:242-250.

Tang, X.Y., Holland, D., et al., 2015. The Diffeomorphometry of Regional Shape Change Rates and its Relevance to Cognitive Deterioration in Mild Cognitive Impairment and Alzheimer's Disease. Human Brain Mapping 36, 2093-2117.

Tu, L.Y., Styner, M., et al., 2018. Skeletal Shape Correspondence Through Entropy. Ieee Transactions on Medical Imaging 37, 1-11.

Tustison, N.J., Cook, P.A., et al., 2014. Large-scale evaluation of ANTs and FreeSurfer cortical thickness measurements. Neuroimage 99, 166-179.

Tward, D.J., Sicat, C.S., et al., 2017. Entorhinal and transentorhinal atrophy in mild cognitive impairment using longitudinal diffeomorphometry. Alzheimers Dement (Amst) 9, 41-50.

van Oostveen, W.M., de Lange, E.C.M., 2021. Imaging Techniques in Alzheimer's Disease: A Review of Applications in Early Diagnosis and Longitudinal Monitoring. International Journal of Molecular Sciences 22.

von Gunten, A., Kovari, E., et al., 2006. Cognitive impact of neuronal pathology in the entorhinal cortex and CA1 field in Alzheimer's disease. Neurobiology of Aging 27, 270-277.

Wolz, R., Heckemann, R.A., et al., 2010. Measurement of hippocampal atrophy using 4D graph-cut segmentation: Application to ADNI. Neuroimage 52, 109-118.

Xie, L., Wisse, L.E.M., et al., 2020. Longitudinal atrophy in early Braak regions in preclinical Alzheimer's disease. Human Brain Mapping 41, 4704-4717.

Zeng, D.B., Li, Q.L., et al., 2020. Hippocampus Segmentation for Preterm and Aging Brains Using 3D Densely Connected Fully Convolutional Networks. Ieee Access 8, 97032-97044.

Zeng, Q.Z., Li, K.C., et al., 2021. Distinct Atrophy Pattern of Hippocampal Subfields in Patients with Progressive and Stable Mild Cognitive Impairment: A Longitudinal MRI Study. Journal of Alzheimers Disease 79, 237-247.

Zhang, L., Mak, E., et al., 2020. Longitudinal trajectory of Amyloid-related hippocampal subfield atrophy in nondemented elderly. Human Brain Mapping 41, 2037-2047.

Zhao, W.N., Wang, X.T., et al., 2019. Trajectories of the Hippocampal Subfields Atrophy in the Alzheimer's Disease: A Structural Imaging Study. Frontiers in Neuroinformatics 13.

Pizer, Stephen M., Junpyo H., Jared V., et al., 2020. Object shape representation via skeletal models (s-reps) and statistical analysis. In Riemannian Geometric Statistics in Medical Image Analysis, pp. 233-271. Academic Press.

Pizer, S.M. et al. (2013). Nested Sphere Statistics of Skeletal Models. In: Breuß, M., Bruckstein, A., Maragos, P. (eds) Innovations for Shape Analysis. Mathematics and Visualization. Springer, Berlin, Heidelberg.

Siddiqi, Kaleem, Pizer, Stephen M., 2008. Medial Representations. Springer Netherlands.

Miolane, N. , Caorsi, M. , Lupo, U., et al. 2021. ICLR 2021 Challenge for Computational Geometry & Topology: Design and Results.

Eugene, E., 2007. Randomization tests, fourth edition. Crc Press.

Marozzi, M., 2007. Some remarks about the number of permutations one should consider to perform a permutation test. statistica, 64(1), 193-201.

Vogel, J. W., La Joie, R., Grothe, M. J., Diaz-Papkovich, A., Doyle, A., Vachon-Presseau, E., . . . Evans, A. C. (2020). A molecular gradient along the longitudinal axis of the human hippocampus informs large-scale behavioral systems. Nat Commun, 11(1), 960.

Witter, M. P., Amaral, D. G., 2004. Hippocampal Formation.

Figure Legends

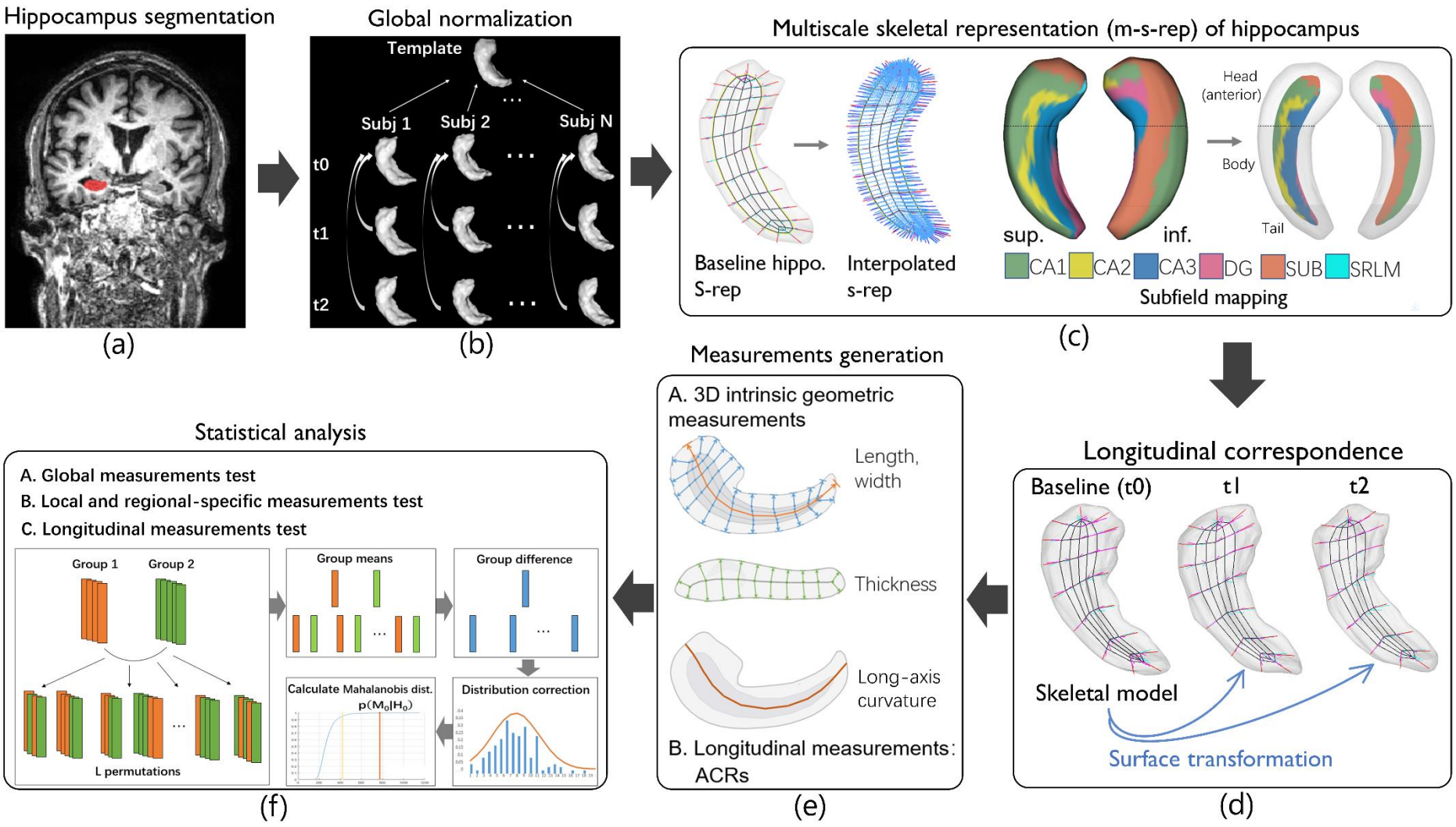
Hippocampus segmentation
Global normalization
Template
Subj 1
Subj 2
Subj N
t0
t1
t2
(a)
(b)
Multiscale skeletal representation (m-s-rep) of hippocampus
Baseline hippo. S-rep
Interpolated s-rep
Head (anterior)
Body
Tail
sup.
inf.
CA1 CA2 CA3 DG SUB SRLM
Subfield mapping
(c)
Longitudinal correspondence
Baseline (t0)
t1
t2
Skeletal model
Surface transformation
(d)
Measurements generation
A. 3D intrinsic geometric measurements
Length, width
Thickness
Long-axis curvature
B. Longitudinal measurements: ACRs
(e)
Statistical analysis
A. Global measurements test
B. Local and regional-specific measurements test
C. Longitudinal measurements test
Group 1
Group 2
L permutations
Group means
Group difference
Calculate Mahalanobis dist.
Distribution correction
(f)

Figure 1. The modelling and analysis pipeline for the hippocampal atrophy evaluation. The raw MRI T1-w images are segmented the hippocampi (a) and globally normalized (b). Then the baseline hippocampi are represented by m-s-reps (c). Longitudinal hippocampi are modelled by m-s-reps, with intra-subject correspondence improved by a deformation-based method (d). The hippocampal atrophy can be characterized by both local and regional-specific spatiotemporal measurements (e). Finally, the measurements are tested AD-sensitivity based on a permutation test method (f). Abbreviations: ACR, annualized change rate; CA, cornu ammonis; DG, dentate gyrus; Sub, subiculum; SRLM: stratum radiatum and stratum lacunosum-moleculare; sup., superior; inf., inferior.

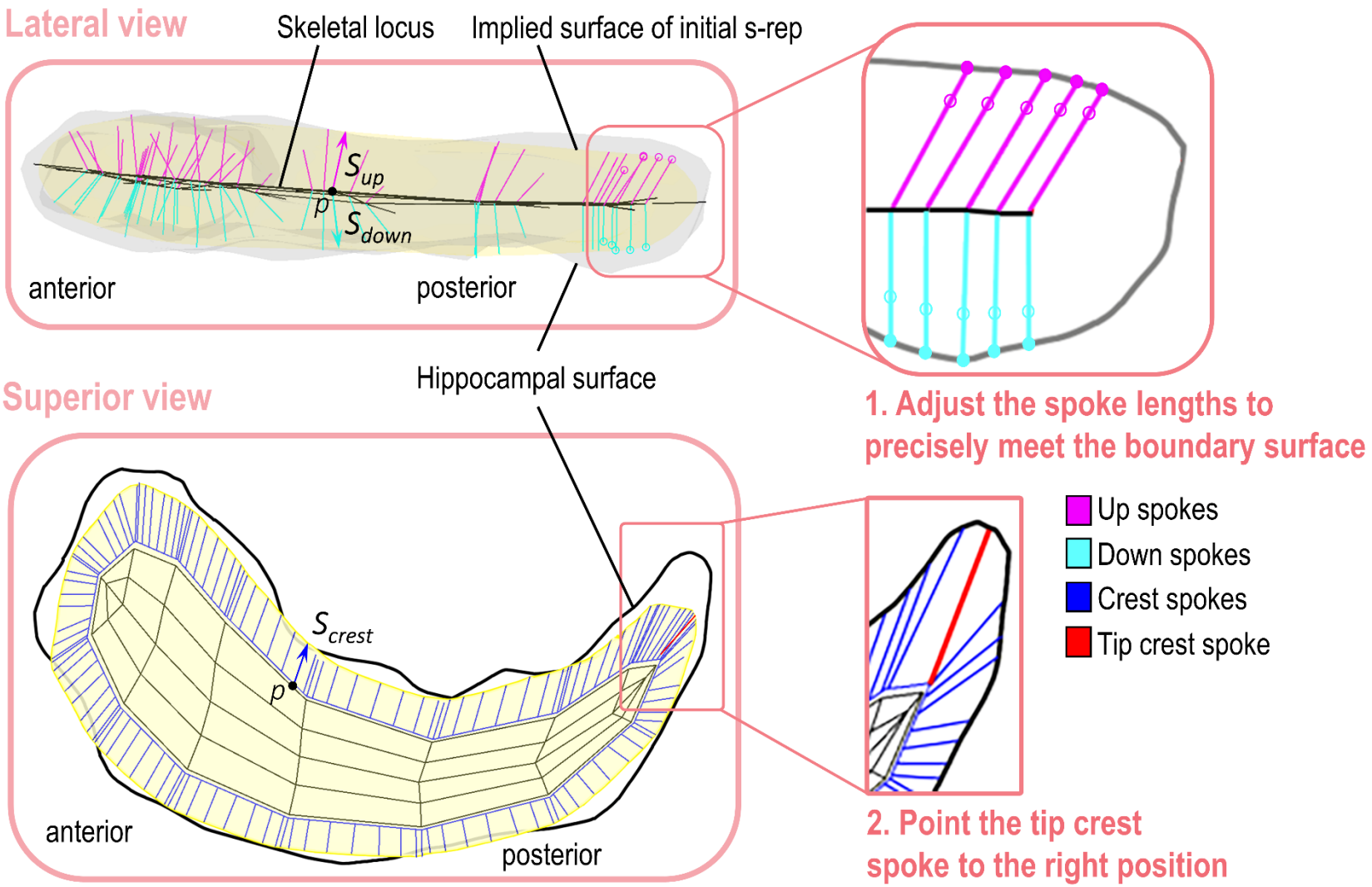
Lateral view
Skeletal locus
Implied surface of initial s-rep
s_{up}
p
s_{down}
anterior
posterior
Hippocampal surface
Superior view
s_{crest}
p
anterior
posterior
1. Adjust the spoke lengths to precisely meet the boundary surface
Up spokes
Down spokes
Crest spokes
Tip crest spoke
2. Point the tip crest spoke to the right position

1

Figure 2. Original s-rep of a hippocampus and its improved s-rep. Left: lateral and superior view of a hippocampus and its initial s-rep (magenta, up spokes; cyan, down spokes; black, skeletal locus; yellow, implied surface). Right: improving the initial s-rep by: 1) adjusting the spoke lengths to precisely meet the boundary surface of the hippocampus (grey) and 2) pointing the tip crest spoke (red) to the right position.

A. Cross-sectional measurements (group comparisons of global and regional measurements: volume, length, LA curvature, width and thickness on each time point)

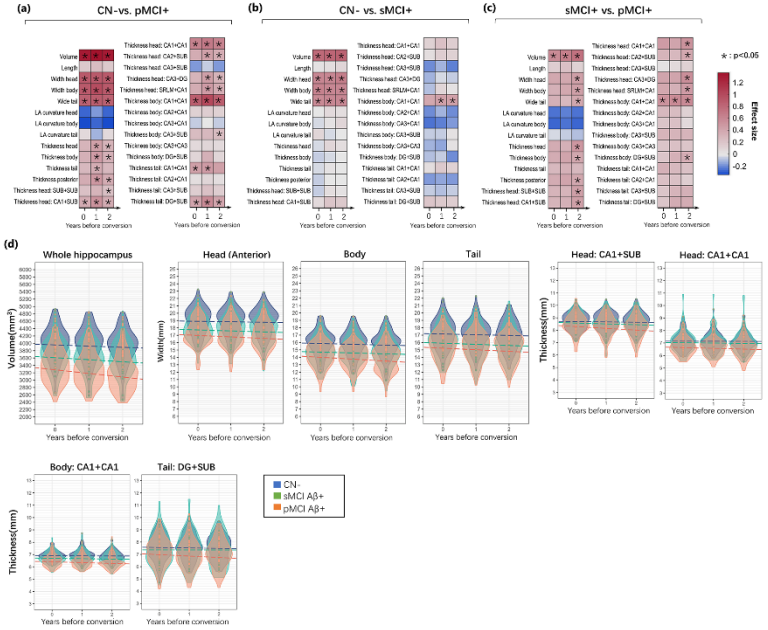

B. Longitudinal measurements (Annualized atrophy rate(%/year) of global and regional measurements)

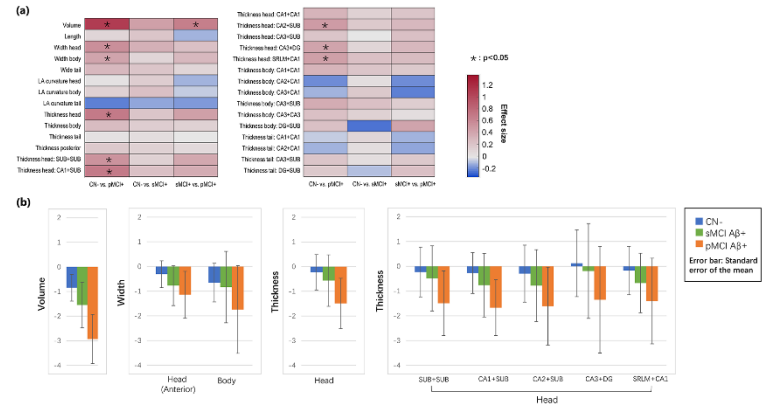

Figure 3. Statistical analysis results of regional atrophy of left hippocampus during the last two years of pMCI-to-AD conversion. A. Between-group comparisons results on cross-sectional measurements. Upper panel: the significance of group comparisons (crimson, $p<<0.05$; yellow, $p=0.05$; grey, $p>0.05$). The effect size using D is shown as color bar, and the p value < 0.05 is marked by star. Figure 3c shows means and standard deviations by violin plots, and trajectories of the measurements by line graphs using linear regression to see the changes of each group over time. Because we focus on features sensitive to diseases at early stage of disease and change over time, only the measurements show significant group difference at all time points are depicted. Note that the significant difference observed in regional long-axis curvatures have positive MDs, suggesting that one group of hippocampi are more curved than the other group along the anterior-posterior dimension of the hippocampus due to the uneven atrophy. B. Means and standard errors of longitudinal measurements for each group, and significance between groups. Abbreviations: pMCI+, Amyloid-β positive progressive mild cognitive impairment; sMCI+, Amyloid-β positive stable mild cognitive impairment; CN, cognitive normal; LA curvature, long-axis curvature.

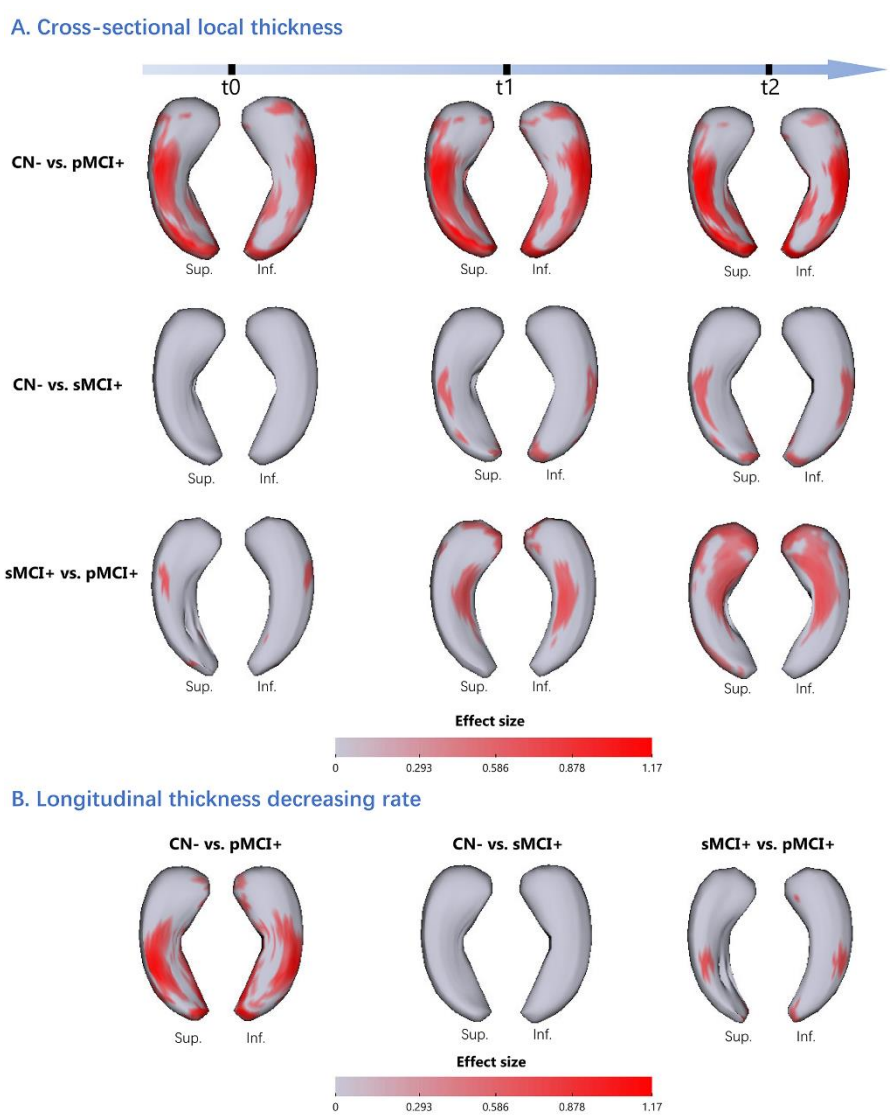
A. Cross-sectional local thickness
t0
t1
t2
CN- vs. pMCI+
CN- vs. sMCI+
sMCI+ vs. pMCI+
Sup.
Inf.
Effect size
0
0.293
0.586
0.878
1.17
B. Longitudinal thickness decreasing rate
CN- vs. pMCI+
CN- vs. sMCI+
sMCI+ vs. pMCI+
Sup.
Inf.
Effect size
0
0.293
0.586
0.878
1.17

1

Figure 4. Statistical analysis results of local thickness of left hippocampus during the last two years of pMCI-to-AD conversion. A. between-group comparisons results on local thickness at each time point (t0, t1, t2). Upper: the significance of pMCI and CN comparison at each time point, colored by p-values. Lower: thickness means differences (MD) of cross-sectional comparisons, colored by MDs of pMCI-CN (red, MD<0; grey, MD>=0). B. between-group comparisons results for annualized thickness decreasing rate. Upper: the significance of pMCI vs. CN, sMCI vs. CN and pMCI vs. sMCI comparisons, colored by p-values. Lower: thickness decreasing rate means differences (MD) of cross-sectional comparisons, colored by MDs of pMCI-CN (red, MD<0; grey, MD>=0).

A. Cross-sectional measurements (group comparisons of global and regional measurements: volume, length, LA curvature, width and thickness on each time point)

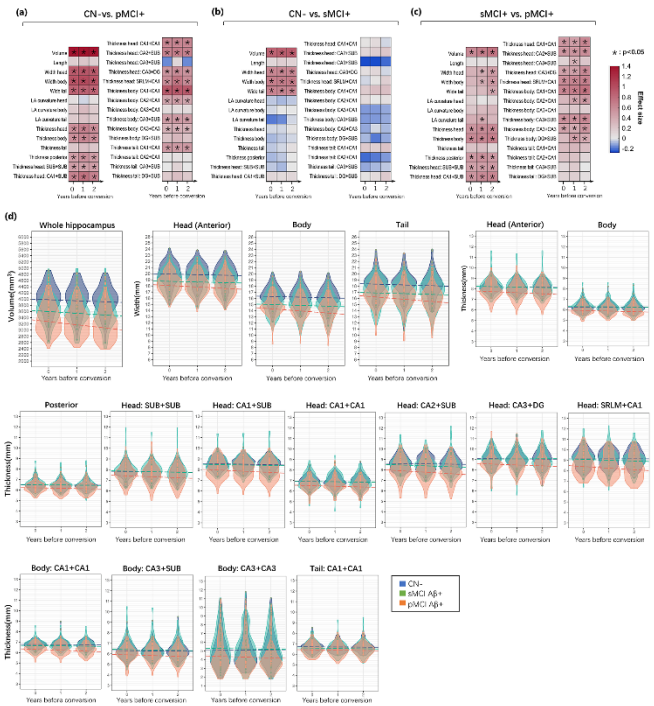

B. Longitudinal measurements (Annualized atrophy rate(%/year) of global and regional measurements)

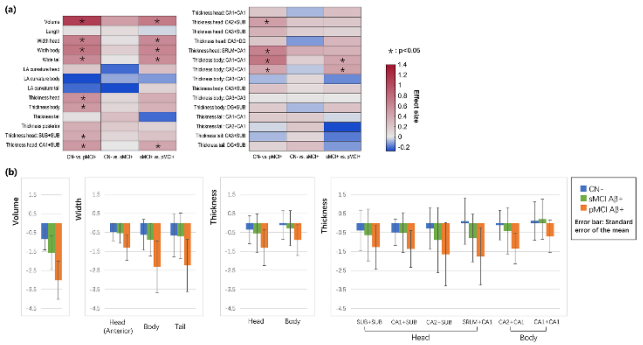

Figure 5. Statistical analysis results of regional atrophy of right hippocampus during the last two years of pMCI-to-AD conversion. A. Between-group comparisons results on cross-sectional measurements. Upper panel: the significance of group comparisons (crimson, $p<<0.05$; yellow, $p=0.05$; grey, $p>0.05$). The effect size using D is shown as color bar, and the p value < 0.05 is marked by star. Figure 3c shows means and standard deviations by violin plots, and trajectories of the measurements by line graphs using linear regression to see the changes of each group over time. Because we focus on features sensitive to diseases at early stage of disease and change over time, only the measurements show significant group difference at all time points are depicted. Note that the significant difference observed in regional long-axis curvatures have positive MDs, suggesting that one group of hippocampi are more curved than the other group along the anterior-posterior dimension of the hippocampus due to the uneven atrophy. B. Means and standard errors of longitudinal measurements for each group, and significance between groups. Abbreviations: pMCI+, Amyloid-β positive progressive mild cognitive impairment; sMCI+, Amyloid-β positive stable mild cognitive impairment; CN, cognitive normal; LA curvature, long-axi

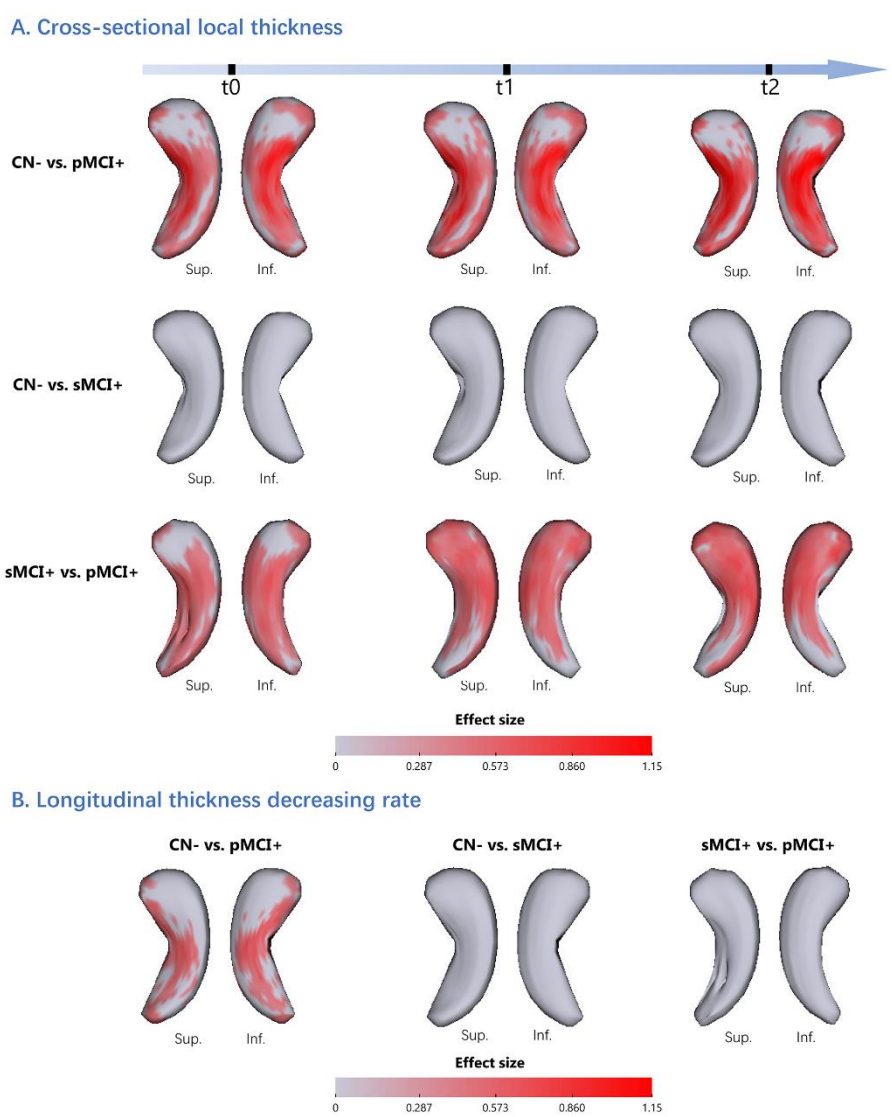
A. Cross-sectional local thickness
t0
t1
t2
CN- vs. pMCI+
CN- vs. sMCI+
sMCI+ vs. pMCI+
Sup.
Inf.
Effect size
0
0.287
0.573
0.860
1.15
B. Longitudinal thickness decreasing rate
CN- vs. pMCI+
CN- vs. sMCI+
sMCI+ vs. pMCI+
Sup.
Inf.
Effect size
0
0.287
0.573
0.860
1.15

1

Figure 6. Statistical analysis results of local thickness of right hippocampus during the last two years of pMCI-to-AD conversion. A. between-group comparisons results on local thickness at each time point (t0, t1, t2). Upper: the significance of pMCI and CN comparison at each time point, colored by p-values. Lower: thickness means differences (MD) of cross-sectional comparisons, colored by MDs of pMCI-CN (red, MD<0; grey, MD>=0). B. between-group comparisons results for annualized thickness decreasing rate. Upper: the significance of pMCI vs. CN, sMCI vs. CN and pMCI vs. sMCI comparisons, colored by p-values. Lower: thickness decreasing rate means differences (MD) of cross-sectional comparisons, colored by MDs of pMCI-CN (red, MD<0; grey, MD>=0).

s curvature.

Table 1. Demographic information for the baseline data enrolled in this study.

	CN Aβ-	sMCI Aβ+	pMCI Aβ+
Number of subjects	81	88	67
Gender (male/female)	43/38	55/33	42/25
Age (years)	75.06±5.1	75.15±7.22	4/96±6.38
Education (years)	16.73±2.54	16.42±2.96	16.10±2.71
MMSE	29.12±1.11	28.32±1.77 *	27.31±1.89 *

Notes: Group difference associated with gender was detected using chi-square test, group differences associated with age, education and neuropsychological sores were detected using non-parametric Kruskal-Wallis test. Data of age, education and MMSE are presented in mean ± standard deviation mode.

*$p < 0.05$; MMSE, Mini-Mental State Examination.

Table 2. Global shape hypothesis test results using the non-Euclidean hypothesis test.

Experiment groups	Left/Right hippocampus		t0	t1	t2
CN vs. pMCI	Left	p-values	0	0	0
		statistics*	4948.910	5232.854	5560.110
	Right	p-values	0	0	0
		Statistics**	5642.559	5573.506	5610.743
CN vs. sMCI	Left	p-values	0.010	0.006	0.002
		statistics*	2273.496	2376.276	3208.199
	Right	p-values	0	0	0.0002
		Statistics**	4368.167	5720.886	3157.594
sMCI vs. pMCI	Left	p-values	0.1860	0.0428	0.0326
		Statistics*	528.202	1230.866	1103.784
	Right	p-values	0.002	0.0001	0
		Statistics**	2217.153	3717.612	5122.539

Note: * The Mahalanobis distances.